Three-dimensional Simulation of Liquid Sloshing in an Elastic Tank

Youlin Zhang*, Decheng Wan‡

State Key Laboratory of Ocean Engineering, School of Naval Architecture, Ocean and Civil Engineering, Shanghai Jiao Tong University, Collaborative Innovation Center for Advanced Ship and Deep-Sea Exploration, Shanghai 200240, China

*Presenting author: sir.zhyl@163.com

‡Corresponding author: dcwan@sjtu.edu.cn

Abstract

Sloshing in a liquid tank of huge size could potentially induce the structural vibration and fatigue damage. Though many numerous researches of sloshing have been conducted to characterize the impact phenomenon, the problem still remains to be addressed since the neglect of hydro-elastic behaviors of structure which will presence in the real phenomenon. In this paper a hybrid method has been developed to study the three-dimensional (3D) liquid sloshing with the consideration of structural elasticity. The improved moving particle semi-implicit (MPS) method is employed to simulate the evolution of 3D flow. The finite element method (FEM) is employed to calculate the vibration of the flexible tank wall. The MPS and FEM methods are coupled with a partition strategy within the fully Lagrangian system. Then, the sloshing in a 3D elastic tank is numerically investigated and results are compared with those corresponding to a 3D rigid tank. The effects of the structural elasticity on the sloshing behaviors are discussed.

Keywords: Particle method; Moving Particle Semi-Implicit (MPS); finite element method (FEM); Fluid structure interaction (FSI); Sloshing; MLParticle-SJTU solver.

Introduction

Fluid structure interaction (FSI) is omnipresent in nature and in many engineering fields. For instance, the sloshing phenomenon occurred in a partially loaded oil tanker or liquid natural gas ship is a typical FSI problem involving multi-physic, yet interrelated liquid, gas and solid domains interact with each other as a unit [1]. For this intricate problem, it's hard to achieve analytical solution whereas laboratory experiment is limited in scope [2]. Considering the fundamental physics involved in the problem can be obtained by numerical simulations, active numerical researches have been carried out in the field of FSI over the past two decades and multiple numerical models were developed [3].

Conventionally, the FSI problems are solved with the fluid field modeled in an arbitrary-Lagrangian-Eulerian (ALE) formulation while the structure field modeled in a Lagrangian formulation. For this approach, grids are necessary to tessellate the solution domain. As the structure undergoes large deformations, the fluid mesh may get highly distorted, especially for a 3D FSI simulation. Although the re-meshing or mesh-updating techniques can be employed to improve the mesh quality as the solution is advanced, extra charge of computation time is unavoidable [4]. Furthermore, the distorted mesh is detrimental for the accuracy of free surface which plays a crucial role in the sloshing phenomenon.

In the recent decade, the fully Lagrangian approaches for both fluid and structure fields are utilized to model the FSI problems since they are flexible in dealing with structural deformation, tracking of free surface, and without having to cope with the nonlinear convective term which appears in the momentum equation in the Eulerian framework. Till to now, several representative Lagrangian methods, such as the smoothed particle hydrodynamics (SPH) method [5], the particle finite element method (PFEM) [6], the material point method (MPM) [7], etc. have been proposed for fluid domain analysis while the FEM method is employed for the structure domain analysis. According to the prior results, disordered pressure fields of fluid are observed, although these methods have shown the great potential for the practical FSI problems involving with motion of fluid or structure particles, surface waves and water splashing. Comparatively, another representative Lagrangian method, the moving particle semi-implicit (MPS) method which is originally proposed by Koshizuka and Oka for incompressible flow [8], is able to achieve smooth fluid pressure field since lots of improvements were proposed to suppress the numerical unphysical pressure oscillation [9]-[11]. In the nearly few years, the MPS method has been introduced into the FSI problems [12]-[16], and results shown that this method is stable and reasonable accurate for simulating nonlinear FSI problems. Hence, the MPS method is employed for the computation of fluid domain of the FSI problem in this paper.

Indeed, all the aforementioned Lagrangian methods for the FSI problems are implemented within two-dimensional space [17]-[22]. To address the practical FSI problems, it's essential to extend these methods into 3D space. However, it's a time consuming task of simulation while the structural domain is dispersed by grids with the nodes coincide with the fluid particles on the interface. Normally a much larger mesh size compared to the size of fluid particle is accurate enough to simulate the structure field. In the present work, the MPS and FEM coupled method is developed for 3D FSI problems, and an interpolation scheme is proposed for the communication on the isomerous interface where the size of structural boundary grids differs from the size of fluid particles. Then, the MPS-FEM coupled method is applied to the practical problem of violent sloshing flow interacting with elastic tank walls, and influence of structural elasticity on the sloshing phenomenon is comparatively investigated.

Numerical methods

In the present study, the FSI problem is numerically studied by a partitioned coupled approach, of which the flow equations and the structural equations are solved separately. Here, the fluid domain is calculated by our in-house particle solver MLParticle-SJTU [23]-[26] based on improved MPS method and the structural domain is calculated by the FEM method.

Fluid solver based on MPS method

Governing equations for incompressible viscous fluid in Lagrangian system are

$$\nabla \cdot \boldsymbol{V} = 0 \tag{1}$$

$$\frac{D\boldsymbol{V}}{Dt} = -\frac{1}{\rho}\nabla P + \nu\nabla^2\boldsymbol{V} + \boldsymbol{g} \tag{2}$$

where $\boldsymbol{V}$, t, ρ, P, ν and $\boldsymbol{g}$ represent the velocity vector, time, water density, pressure, kinematic viscosity and the gravity acceleration vector, respectively.

In particle method, governing equations should be expressed by the particle interaction models based on the kernel function. Here, the kernel function presented by Zhang et al.[23] is employed.

$$W(r)=\begin{cases}\dfrac{r_e}{0.85r+0.15r_e}-1 & 0\le r<r_e\\ 0 & r_e\le r\end{cases} \tag{3}$$

where r is distance between particles and r_e is the effect radius.

The particle interaction models, including the differential operators of gradient, divergence and Laplacian, are defined as

$$<\nabla\phi>_i=\frac{dim}{n^0}\sum_{j\neq i}\frac{\phi_j+\phi_i}{|\boldsymbol{r}_j-\boldsymbol{r}_i|^2}(\boldsymbol{r}_j-\boldsymbol{r}_i)\cdot W(|\boldsymbol{r}_j-\boldsymbol{r}_i|) \tag{4}$$

$$<\nabla\cdot\boldsymbol{\Phi}>_i=\frac{dim}{n^0}\sum_{j\neq i}\frac{\left(\boldsymbol{\Phi}_j-\boldsymbol{\Phi}_i\right)\cdot\left(\boldsymbol{r}_j-\boldsymbol{r}_i\right)}{|\boldsymbol{r}_j-\boldsymbol{r}_i|^2}W(|\boldsymbol{r}_j-\boldsymbol{r}_i|) \tag{5}$$

$$<\nabla^2\phi>_i=\frac{2dim}{n^0\lambda}\sum_{j\neq i}(\phi_j-\phi_i)\cdot W(|\boldsymbol{r}_j-\boldsymbol{r}_i|) \tag{6}$$

where ϕ is an arbitrary scalar function, $\boldsymbol{\Phi}$ is an arbitrary vector, *dim* is the number of space dimensions, n^0 is the initial particle number density for incompressible flow, λ is a parameter defined as

$$\lambda=\frac{\sum_{j\neq i}W(|\boldsymbol{r}_j-\boldsymbol{r}_i|)\cdot|\boldsymbol{r}_j-\boldsymbol{r}_i|^2}{\sum_{j\neq i}W(|\boldsymbol{r}_j-\boldsymbol{r}_i|)} \tag{7}$$

which is introduced to keep the variance increase equal to that of the analytical solution [8].

The incompressible condition of MPS method is represented by keeping the particle number density constant. In each time step, there are two stages: first, temporal velocity of particles is calculated based on viscous and gravitational forces, and particles are moved according to the temporal velocity; second, pressure is implicitly calculated by solving a Poisson equation, and the velocity and position of particles are updated according to the obtained pressure. The Pressure Poisson Equation (PPE) in present MPS solver is defined as

$$<\nabla^2P^{n+1}>_i=(1-\gamma)\frac{\rho}{\Delta t}\nabla\cdot\boldsymbol{V}_i^*-\gamma\frac{\rho}{\Delta t^2}\frac{<n^*>_i-n^0}{n^0} \tag{8}$$

where γ is a blending parameter with a value between 0 and 1. The range of $0.01\le\gamma\le0.05$ is better according to numerical experiments conducted by Lee et al.[27] In this paper, $\gamma=0.01$ is adopted for all simulations.

For the MPS method, pressure of the fluid domain is closely affected by the accuracy of free surface detection. In present solver, we employ a free surface detection method by Zhang et al.[23] and defined as

$$<\boldsymbol{F}>_i=\frac{dim}{n^0}\sum_{j\neq i}\frac{1}{|\boldsymbol{r}_i-\boldsymbol{r}_j|}(\boldsymbol{r}_i-\boldsymbol{r}_j)W(\boldsymbol{r}_{ij}) \tag{9}$$

where the vector function $\boldsymbol{F}$ represents the asymmetry of arrangements of neighbor particles. Particle satisfying

$$<|\boldsymbol{F}|>_i\ >\ 0.9|\boldsymbol{F}|^0 \tag{10}$$

is considered as free surface particle, where $|\boldsymbol{F}|^0$ is the initial value of $|\boldsymbol{F}|$ for surface particle.

Structure solver based on FEM method

In present study, the FEM method is employed to solve the deformation of structure which is governed by the equations expressed as

$$\mathbf{M}\,\ddot{\boldsymbol{y}} + \mathbf{C}\,\dot{\boldsymbol{y}} + \mathbf{K}\,\boldsymbol{y} = \boldsymbol{F}(t) \tag{11}$$

$$\mathbf{C} = \alpha_1 \mathbf{M} + \alpha_2 \mathbf{K} \tag{12}$$

where **M**, **C**, **K** are the mass matrix, the Rayleigh damping matrix, the stiffness matrix of the structure, respectively. $\boldsymbol{F}$ is the external force vector acting on structure, and varies with computational time. $\boldsymbol{y}$ is the displacement vector of structure. α_1 and α_2 are coefficients which are related with natural frequencies and damping ratios of structure.

To solve the structural dynamic equation, another two group functions should be supplemented to set up a closed-form equation system. Here, Taylor's expansions of velocity and displacement developed by Newmark [28] are employed:

$$\dot{\boldsymbol{y}}_{t+\Delta t} = \dot{\boldsymbol{y}}_t + (1-\gamma)\ddot{\boldsymbol{y}}_t \Delta t + \gamma \ddot{\boldsymbol{y}}_{t+\Delta t}\Delta t \quad , \quad 0<\gamma<1 \tag{13}$$

$$\boldsymbol{y}_{t+\Delta t} = \boldsymbol{y}_t + \dot{\boldsymbol{y}}_t \Delta t + \frac{1-2\beta}{2}\ddot{\boldsymbol{y}}_t \Delta t^2 + \beta \ddot{\boldsymbol{y}}_{t+\Delta t}\Delta t^2 \quad , \quad 0<\beta<1 \tag{14}$$

where β and γ are important parameters of the Newmark method, and selected as β=0.25, γ=0.5 for all simulations in present paper. The nodal displacements at $t = t+\Delta t$ can be solved by the following formula [29]:

$$\bar{\mathbf{K}}\,\boldsymbol{y}_{t+\Delta t} = \bar{\boldsymbol{F}}_{t+\Delta t} \tag{15-a}$$

$$\bar{\mathbf{K}} = \mathbf{K} + a_0\mathbf{M} + a_1\mathbf{C} \tag{15-b}$$

$$\bar{\boldsymbol{F}}_{t+\Delta t} = \boldsymbol{F}_t + \mathbf{M}(a_0\boldsymbol{y}_t + a_2\dot{\boldsymbol{y}}_t + a_3\ddot{\boldsymbol{y}}_t) + \mathbf{C}(a_1\boldsymbol{y}_t + a_4\dot{\boldsymbol{y}}_t + a_5\ddot{\boldsymbol{y}}_t) \tag{15-c}$$

$$\begin{aligned} &a_0 = \frac{1}{\beta\Delta t^2},\ a_1 = \frac{\gamma}{\beta\Delta t},\ a_2 = \frac{1}{\beta\Delta t},\ a_3 = \frac{1}{2\beta}-1, a_4 = \frac{\gamma}{\beta}-1, \\ &a_5 = \frac{\Delta t}{2}(\frac{\gamma}{\beta}-2),\ a_6 = \Delta t(1-\gamma),\ a_7 = \gamma\Delta t \end{aligned} \tag{15-d}$$

where $\bar{\mathbf{K}}$ and $\bar{\boldsymbol{F}}$ are so-called effective stiffness matrix and effective force vector, respectively. Finally, the accelerations and velocities corresponding to the next time step are updated as follows.

$$\ddot{\boldsymbol{y}}_{t+\Delta t} = a_0(\boldsymbol{y}_{t+\Delta t} - \boldsymbol{y}_t) - a_2\dot{\boldsymbol{y}}_t - a_3\ddot{\boldsymbol{y}}_t \tag{16}$$

$$\dot{\boldsymbol{y}}_{t+\Delta t} = \dot{\boldsymbol{y}}_t + a_6\ddot{\boldsymbol{y}}_t + a_7\ddot{\boldsymbol{y}}_{t+\Delta t} \tag{17}$$

Data interpolation on the interface between fluid and structure domain

For the simulation of 3D FSI problems based on aforementioned MPS-FEM coupled method, the space of fluid domain will be dispersed by particles while the space of structural domain will be dispersed by grids. In general, the fine particles should be arranged within the fluid domain to keep a satisfactory precision for the fluid analysis. By contrast, the much coarser grids could be accurate enough for the structure analysis, which indicates that the fluid particles are not coincided with the structural nodes on the interface between the fluid and structure domain. Hence, the isomerous interface between the two domains may result in the challenge of data exchange in the process of FSI simulation. In the present study, special data interpolation technique is implied to apply the external force carried by the fluid particles onto the structural nodes and update the positions of boundary particles corresponding to the displacements of structural nodes.

For the transformation of force from the fluid domain to the structural boundary, the schematic diagram of the technique is shown in Figure 1 and the procedure of interpolation can be summarized as below.

(1) The mapping relationship between the boundary particle and the structural element will be established while the particle is arranged within the element at the initial time instant.

(2) The external force Q_j acting on the structural boundary is calculated by the formula

$$Q_j = P_j \cdot l_0^2 \quad (i = 1,2,3,4;\ j = 1,2\cdots npe) \tag{18}$$

where P_j is the pressure of the boundary particle obtained from the fluid domain, l_0 is the initial distance between neighbor particles, *npe* is the number of particles on the interface.

(3) The force Q_j carried by the boundary particle *j* is divided into four parts and assigned onto the four nodes of the element *s* by the formula (19) with the help of the interpolation vector $\boldsymbol{N}$, which is consisted of the shape functions N_k, N_{xk}, N_{yk}.

$$\boldsymbol{F}_s^e = [\boldsymbol{F}_{s,1}^e\ \boldsymbol{F}_{s,2}^e\ \boldsymbol{F}_{s,3}^e\ \boldsymbol{F}_{s,4}^e] = \boldsymbol{N}^{\mathrm{T}} Q_j \ \ (s = 1,2\cdots ne) \tag{19}$$

$$\boldsymbol{N} = \begin{bmatrix} N_1 & N_{x1} & N_{y1} & N_2 & N_{x2} & N_{y2} & N_3 & N_{x3} & N_{y3} & N_4 & N_{x4} & N_{y4} \end{bmatrix} \tag{20}$$

$$\begin{aligned} N_k &= \frac{1}{8}\left(1+\xi_k\xi\right)(1+\eta_k\eta)(2+\xi_k\xi+\eta_k\eta-\xi^2-\eta^2) \\ N_{xk} &= -\frac{1}{8}b\eta_k\left(1+\xi_k\xi\right)(1+\eta_k\eta)(1-\eta^2) \\ N_{yk} &= \frac{1}{8}a\xi_k\left(1+\xi_k\xi\right)(1+\eta_k\eta)(1-\xi^2) \end{aligned} \tag{21}$$

$$\xi = \frac{x}{a}, \xi_k = \frac{x_k}{a}, \eta = \frac{y}{b}, \eta_k = \frac{y_k}{b} \quad (k = 1,2,3,4) \tag{22}$$

where $\boldsymbol{F}_s^e$ is the force vector regarding the element *s*, *a* and *b* are the half values of the width and height of the element, respectively.

(4) Finally, the equivalent nodal force $\boldsymbol{F}_I$ corresponding to the node *I* is obtained by the summation of force components regarding to the four neighbor elements.

$$\boldsymbol{F}_I = \boldsymbol{F}_{r,3} + \boldsymbol{F}_{s,4} + \boldsymbol{F}_{m,1} + \boldsymbol{F}_{n,2} \tag{23}$$

where $\boldsymbol{F}_{s,4}$ is the force component contributed by the element *s*. Schematic program of the neighbor elements adjoining the node *I* and the concept of nodes numbering within element are shown as Figure 2.

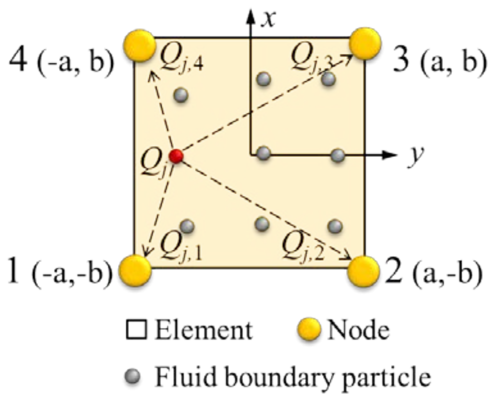

Figure 1.Schematic program of the force interpolation within element

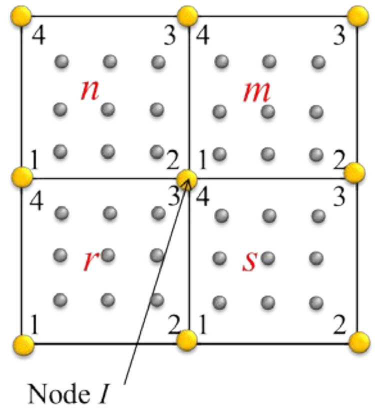

Figure 2. Schematic program of the neighbor elements adjoining the node I

Besides, the fluid boundary which is consisted of particles will deforms corresponding to the deformation of structural boundary. The deflection values of boundary particles *w* can be obtained by the interpolation based on the shape functions ***N*** and the nodal displacements $\boldsymbol{\delta}$.

$$w = \boldsymbol{N}\boldsymbol{\delta} \tag{24}$$

$$\boldsymbol{\delta} = [w_1 \quad \theta_{x1} \quad \theta_{y1} \quad w_2 \quad \theta_{x2} \quad \theta_{y2} \quad w_3 \quad \theta_{x3} \quad \theta_{y3} \quad w_4 \quad \theta_{x4} \quad \theta_{y4}]^{\mathrm{T}} \tag{25}$$

where w_i is the linear displacement of node ***i***, θ_{xi} and θ_{yi} are the angular displacements around the axis *x* and *y*, respectively.

Numerical Simulations

In the ship and ocean engineering, the sloshing phenomenon in a partially filled liquid tank is of great importance in assessing the strength of structure and has been intensively studied in the past a few decades. However, most contributions are focused on the mechanism of the nonlinear phenomenon regarding the rigid tank, and the elasticity of tank walls, which plays an important role in the sloshing phenomenon, have not been taken into account.

In this study, the aforementioned MPS-FEM coupled method is employed to simulate the interaction between sloshing flow and three dimensional elastic tank. The influence of structural elasticity on the sloshing phenomenon will be investigated by comparing against the phenomenon in a rigid tank.

Numerical setup

Figure 3 shows the schematic diagram of the 3D computational model. The tank is free to roll around the axis *O-O'* which is the symmetry axis of the floor. The tank is forced to roll harmoniously with the governing equation of motion defined as

$$\theta(t) = \theta_0 \sin(\omega t) \tag{10}$$

where $\theta(t)$ is the rotation angle of the tank, the excitation amplitude θ_0 is set to 4 degrees, the angular frequency of rotation ω is set to 3.857 rad/s. To investigate the climb of water on the lateral wall of tank, the wave probe is mounted at the point A (0.01, 0, 0). In addition, the vibration of left lateral wall will be measured at the point B (0, 0.05, 0), C (0, 0.08, 0), E (0, 0.15, 0), F (0, 0.2, 0), and the impact pressure will be recorded at the point D (0, 0.095, 0).

In the present simulations, the 3D computational model is dispersed by particles with an initial spacing size (l_0) of 0.005 m for both rigid and elastic tanks. To calculate the structural responses of the elastic walls which would experience the sloshing impact loads, the lateral tank walls are dispersed by elements with the spacing size of 0.01 m. Detailed parameters for both fluid and structural analysis are presented in Table 1. Herein, the Rayleigh's damping has been taken into account for the structural analysis by setting the factor of mass-proportional contribution α_1 as 0.0128 while the factor of stiffness-proportional contribution α_2 as 5.01e^{-7}.

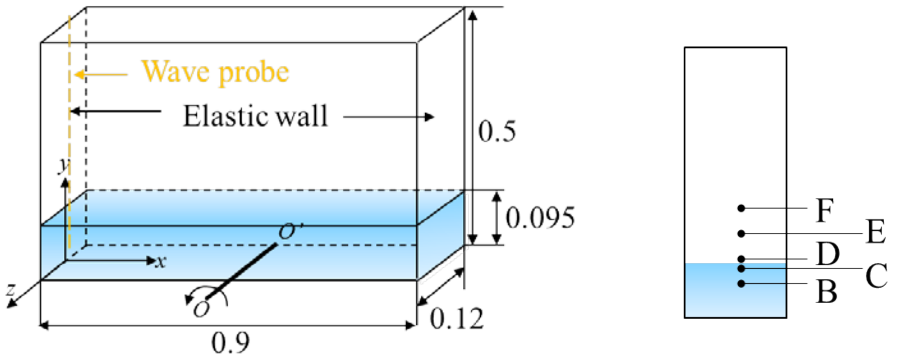

(a) tank (b) measuring points

Figure 3. Schematic diagram of the rolling tank with elastic lateral walls (Unit: m)

Table 1. Simulation parameters of numerical cases

Fluid parameters	Values	Structural parameters	Values
Fluid density (kg/m^3)	1000	Structure density (kg/m^3)	1800
Kinematic viscosity (m^2/s)	5×10^{-5}	Young's modulus (GPa)	10
Gravitational acceleration (s/m^2)	9.81	Poisson's ratio	0.3
Particle spacing (m)	0.005	Element size (m)	0.01
Number of fluid particles	74106	Damping coefficients α_1	0.025
Total number of particles	229816	Damping coefficients α_2	0.0005
Time step size (s)	1×10^{-4}	Time step size (s)	1×10^{-4}

Impact loads on lateral walls

The elasticity of tank walls can give rise to the difference of the impact loads acting on the lateral walls between the elastic and rigid tanks. As shown in Figure 4, the pressure time histories corresponding to rigid tank and elastic tank are measured at the point D. For the pressure in a rigid tank, the well-known character of the impact events, "church roof shape", is observed. For the pressure in the tank with elastic lateral walls, the roof shape of the impact pressure signal shows much different features comparison against that regarding rigid tank. For instance, the peaks of the impact pressure are less than 2200 Pa, which are obviously smaller than those regarding the rigid tank. Furthermore, the pressure curve presents much larger amplitude oscillation, as shown in Figure 4 (b). According to the enlarged signal of pressure, four peaks and three valleys can be observed within one cycle of tank's roll motion. The oscillation of pressure should be closely linked to the vibration of elastic wall.

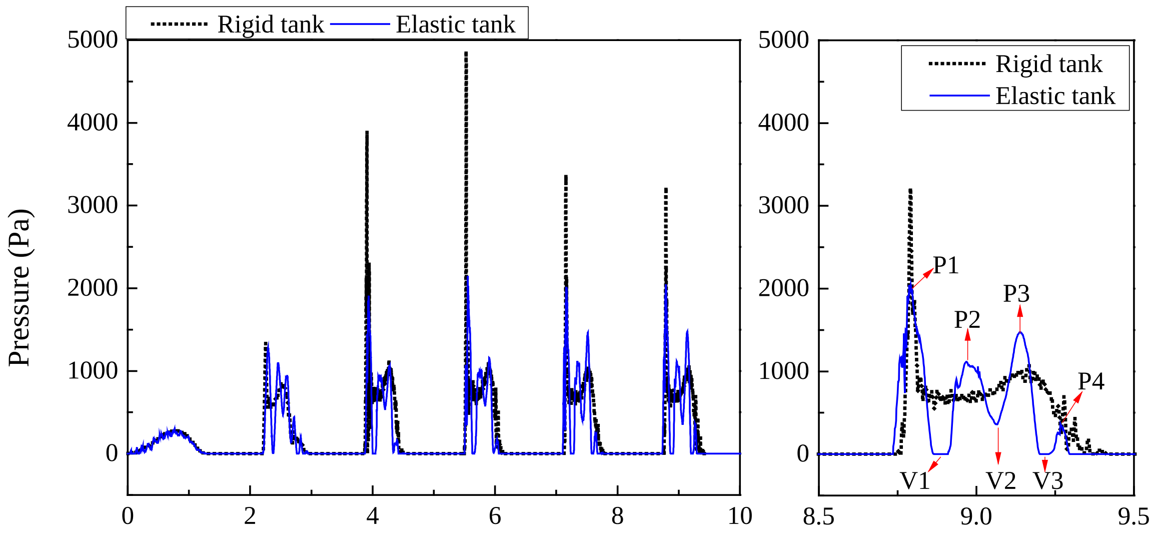

(a) whole signal (b) enlarged signal

Figure 4. Time histories of pressure at the measuring point D

Climb of water front on lateral walls

The elasticity of tank walls can also lead to the difference of free surface evolutions between the elastic and rigid tanks. Figure 5 shows the time histories of water levels at the measuring point A. According to the figure, the water level regarding the elastic tank is much lower than that of rigid tank. Herein, the water level corresponding to the rigid tank is marked as "level 1" with the value 0.335 m, and the peaks of the curve is 0.5 m which indicates that the water particles hit the roof at a certain time instant since the splashing of water front. In contrast, the water level regarding the elastic tank is marked as "level 2" with the value 0.24 m, and the curve is featured with no pulsing signal which indicates that the splashing phenomenon of water front would not be observed in the region above the measuring point.

Figure 6 shows the climbs of water fronts on the lateral walls in the front view. At the instant t_1, the fluid particles distribute evenly over the rigid wall after the front of sloshing wave impacting onto the lateral wall, while those cluster at the area A with the shape "O" on the elastic wall. At the instant $t_2 = t_1+0.1$ s, the jet water climbs along the rigid wall and the distribution of fluid particles is homogeneous in the z direction. In contrast, the distribution of jet water along the elastic wall is uneven and presents in the "V" form.

To obtain a more clear understanding of the difference of the free surface between the elastic and rigid tanks, the climbs of water fronts on the lateral walls are shown as Figure 7 in the side view. At the instant t_1, the jet is generated after the impact event and turns to climb upward along the rigid wall. In comparison, the direction of the jet water inclines to inside of the tank since the deformation of the wall. At the instant t_2, the water front regarding the rigid wall climbs up to roof of the tank without gap between the water surface and the lateral wall. However, the triangular pocket may exist at the upper corner of the elastic tank while the free surface touches the roof.

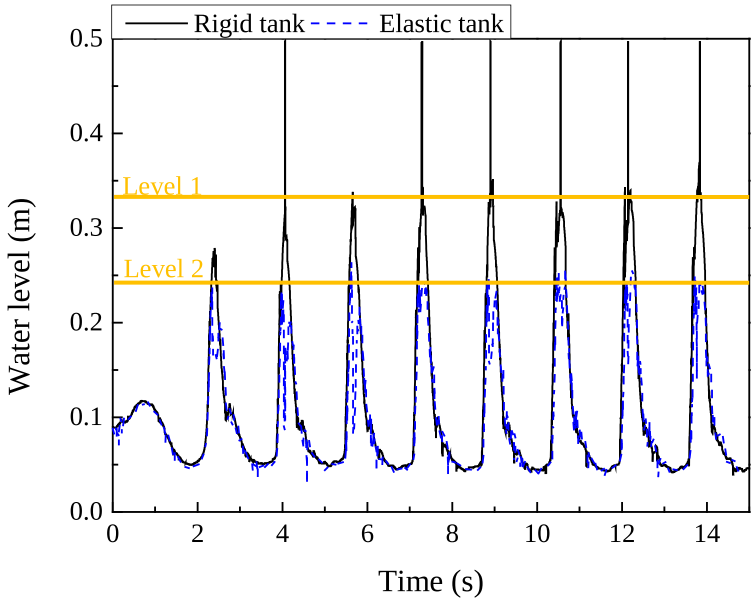

Figure 5. Evolution of water level at point A

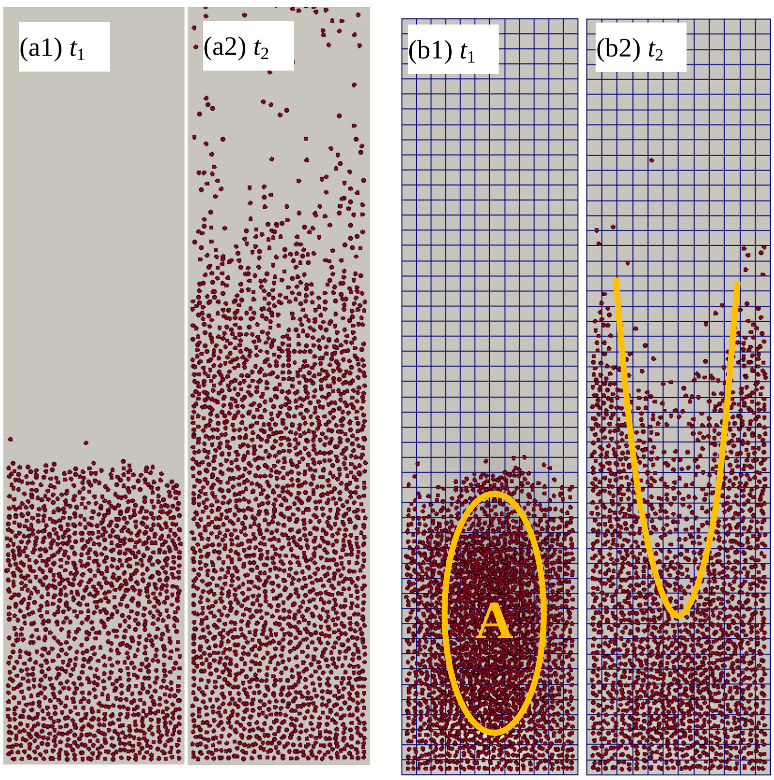

(a) Rigid tank (b) Elastic tank

Figure 6. Climb of water front on the lateral wall (front view)

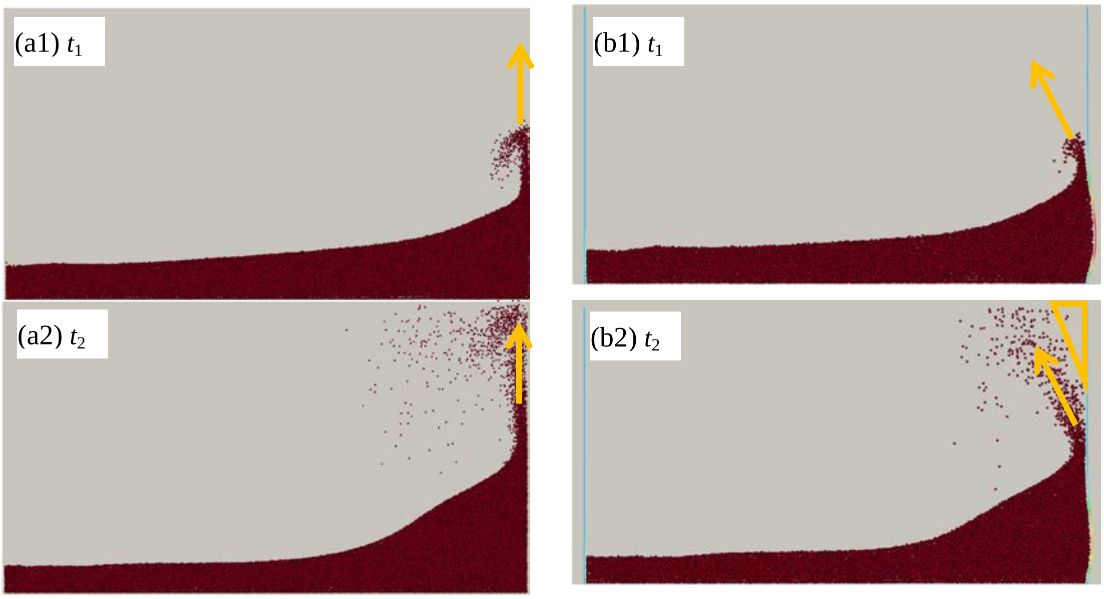

(a) Rigid tank (b) Elastic tank

Figure 7. Climb of water front on the lateral wall (side view)

Deformation of elastic walls

Figure 8 shows the time histories of displacements of measuring points which mounted on left wall of the elastic tank. The similar character of the structural oscillations regarding different measuring points can be observed. According to the trends of the curves, the large amplitude vibrations present periodically and following with small amplitude vibrations. Remarkably, the oscillation amplitude of the measuring point C is much larger than that of other points away from it, which proofs that the elastic wall deforms with 3D feature, as exhibited in Figure 9.

Figure 10 shows the relationship between structural vibration and impact pressure. Herein, the time instant when the pressure going up drastically is marked as t_{impact} which denotes the start of the sloshing impact event, and the time instant when the pressure drops to zero is marked as t_{end} which denotes the end of the impact event. The trend of pressure is in gear with that of structural vibration during the impact stage, which indicates that the impact pressure is sensitive to the vibration of tank wall. It can be inferred that the fluid particles may be drove away from the elastic wall and a gap would generate between the fluid and the lateral wall during the interaction of sloshing flow and the tank. As a result, the pressure which is measured by the contribution of neighbor fluid particles would rapidly reduce and result in the valleys of the pressure signal. In addition, the elastic wall vibrates with the amplitude decreasing gradually beyond the impact stage, which is induced by the joint effects of the structural damping and elastic restoring force.

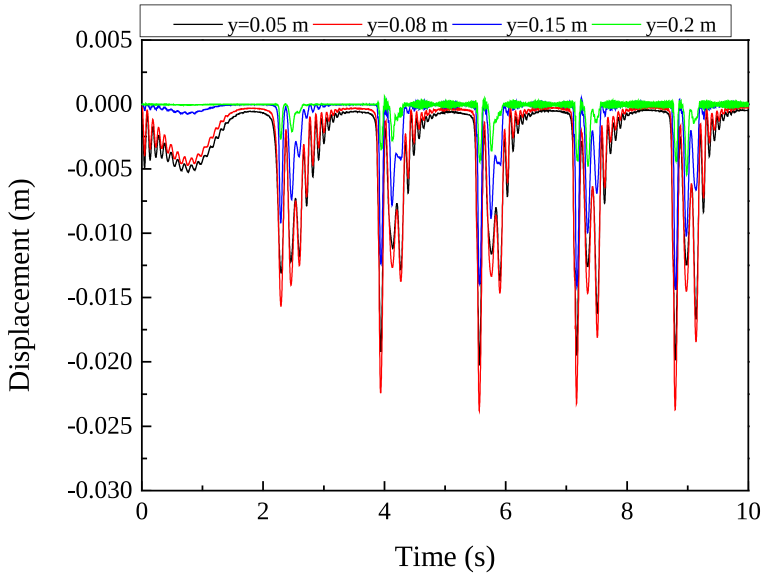

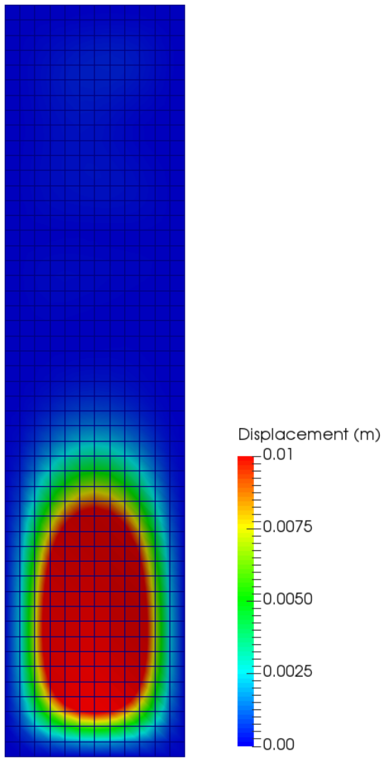

Figure 8. **Time history of structural displacement at measuring points B, C, D and E**

Figure 9. **Deformation of elastic wall**

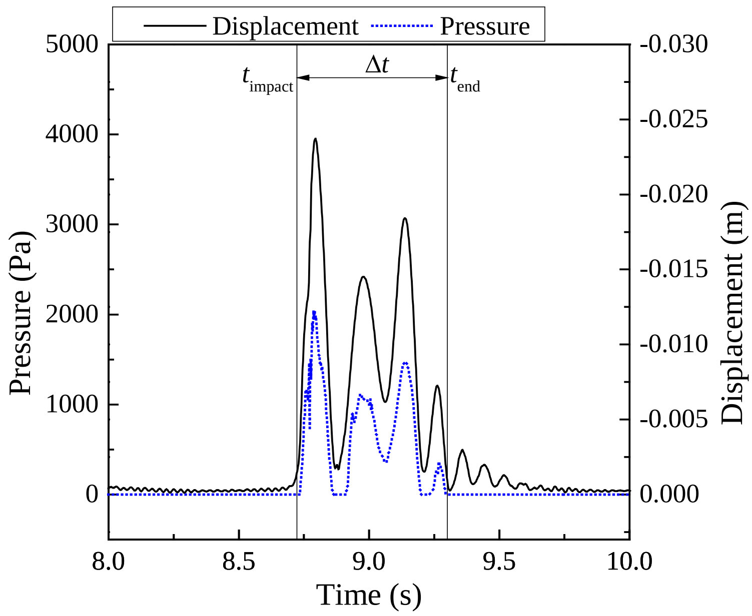

Figure 10. **Relationship between structural vibration and impact pressure**

Conclusions

In the present study, the in-house solver MLParticle-SJTU based on the MPS-FEM coupled method is developed for 3D FSI problems. The mathematical equations for the MPS and FEM methods are introduced and an interface interpolation approach for data transformation between fluid and structure domains is proposed. With the help of the present FSI solver, the tentative investigation of 3D sloshing problem with the consideration of structural deformation can be successfully conducted. According to the numerical results, the influence of structural elasticity on the sloshing phenomenon can be observed. For instance, the elasticity of tank wall can give rise to the large amplitude oscillation of pressure which is in gear with that of structural vibration during the impact event. The lateral wall deforms in the form of cambered surface while the sloshing wave impacting onto it. The climb height of water front on the elastic wall is much lower than that regarding the rigid tank. The particle distribution of jet water presents the "V" form over the elastic wall while that is homogeneous over the rigid wall. Generally, the study present in this paper shows that the present MPS-FEM coupled method is a promising numerical tool for simulating highly non-linear liquid sloshing in an elastic tank.

Acknowledgement

This work is supported by the National Natural Science Foundation of China (51379125, 51490675, 11432009, 51579145), Chang Jiang Scholars Program (T2014099), Shanghai Excellent Academic Leaders Program (17XD1402300), Program for Professor of Special Appointment (Eastern Scholar) at Shanghai Institutions of Higher Learning (2013022), Innovative Special Project of Numerical Tank of Ministry of Industry and Information Technology of China (2016-23/09) and Lloyd's Register Foundation for doctoral student, to which the authors are most grateful.

References

[1] Landajuela, M., Vidrascu, M., Chapelle, D. and Fernandez, M. A. (2017) Coupling schemes for the FSI forward prediction challenge: comparative study and validation, *International Journal for Numerical Methods in Biomedical Engineering*, e02813.

[2] Hou, G., Wang, J. and Layton, A. (2012) Numerical methods for fluid-structure interaction-A review, *Commun. Comput. Phys.* **12** (2), 337–377.

[3] Ryzhakov, P. (2017) A modified fractional step method for fluid–structure interaction problems, *Revista Internacional de Métodos Numéricos para Cálculo y Diseño en Ingeniería* **33**(1), 58–64.

[4] Farahani, M. H., Amanifard, N. and Hosseini, S. M. (2009) A Fluid-Structure Interaction Simulation by Smoothed Particle Hydrodynamics, *Engineering Letters* **17**(1), 30–35.

[5] Monaghan, J. J. (1994) Simulating Free Surface Flows with SPH, *Journal of Computational Physics* **110**(2), 399–406.

[6] Idelsohn, S. R., Onate, E. and Del, P. F. (2004) The Particle Finite Element Method: A Powerful tool to Solve Incompressible Flows with Free-surfaces and Breaking Waves, *International Journal for Numerical Methods in Engineering* **61**(7), 964–989.

[7] Li, J. G., Hamamoto, Y., Liu, Y. and Zhang, X. (2014) Sloshing impact simulation with material point method and its experimental validations, *Computers & Fluids* **103**, 86–99.

[8] Koshizuka, S. and Oka, Y. (1996) Moving particle semi-implicit method for fragmentation of incompressible fluid, *Nuclear Science and Engineering* **123**, 421–434.

[9] Khayyer, A. and Gotoh, H. (2011) Enhancement of stability and accuracy of the moving particle semi-implicit method, *Journal of Computational Physics* **230**, 3093–3118.

[10] Khayyer, A. and Gotoh, H. (2013) Enhancement of performance and stability of MPS mesh-free particle method for multiphase flows characterized by high density ratios, *Journal of Computational Physics* **242**, 211–233.

[11] Khayyer, A., Gotoh, H. and Shimizu, Y. (2017) Comparative study on accuracy and conservation properties of two particle regularization schemes and proposal of an optimized particle shifting scheme in ISPH context, *Journal of Computational Physics* **332**, 236–256.

[12] Zhang, Y. L., Tang, Z. Y. and Wan, D. C. (2016) *MPS-FEM Coupled Method for Interaction between Sloshing Flow and Elastic Structure in Rolling Tanks*, Proceedings of the 7th International Conference on Computational Methods (ICCM2016), Berkeley, USA, 1493-6106-1-PB.

[13] Zhang, Y. L., Chen, X. and Wan, D. C. (2016) MPS-FEM coupled method for the comparison study of liquid sloshing flows interacting with rigid and elastic baffles, *Applied Mathematics and Mechanics* **37**(12), 1359–1377. (In Chinese)

[14] Zhang, Y. L., Chen, X. and Wan, D. C. (2016) *Simulation of Dam-Break Flow Interaction with Elastic Gate by MPS-FEM Coupled Method*, Proceedings of the 11th Asian Computational Fluid Dynamics Conference (ACFD2016), Dalian, China, 390–394.

[15] Mitsume, N., Yoshimura, S., Murotani, K. and Yamada, T. (2014a) MPS-FEM partitioned coupling approach for fluid-structure interaction with free surface flow, *International Journal of Computational Methods* **11**(4), 4157–4160.

[16] Mitsume, N., Yoshimura, S., Murotani, K. and Yamada, T. (2014b) Improved MPS-FE Fluid-Structure Interaction Coupled Method with MPS Polygon Wall Boundary Model, *Comput. Model. Eng. Sci* **101**(4), 229–247.

[17] Liao, K. P. and Hu, C. H. (2013) A coupled FDM-FEM method for free surface flow interaction with thin elastic plate, *J. Mar. Sci. Technol* **18**, 1–11.

[18] Hou, G., Wang, J. and Layton, A. (2012) Numerical Methods for Fluid-Structure Interaction - A Review, *Commun. Comput. Phys* **12**(2), 337–377.

[19] Longatte, E., Verremana, V. and Souli, M. (2009) Time marching for simulation of fluid-structure interaction problems, *Journal of Fluids and Structures* **25**, 95–111.

[20] Sun, Z., Xing, J. T., Djidjeli, K. and Cheng, F. (2015) *Coupling MPS and Modal Superposition Method for Flexible Wedge Dropping Simulation*, Proceedings of the Twenty-fifth International Ocean and Polar Engineering Conference, Kona, Big Island, Hawaii, USA, 144–151.

[21] Onate, E., Idelsohn, S. R., Celigueta, M. A. and Rossi, R. (2006) *Advances in the particle finite element method for fluid-structure interaction problems*, Proceedings of 1st South-East European Conference on Computational Mechanics (SEECCM-06), Kragujevac, Serbia and Montenegro.

[22] Idelsohn, S. R., Marti, J., Limache, A. and Onate, E. (2008) Unified Lagrangian formulation for elastic solids and incompressible fluids: Application to fluid-structure interaction problems via the PFEM, *Comput. Methods Appl. Mech. Eng* **197**, 1762–1776.

[23] Zhang, Y. X., Wan, D. C. and Hino, T. (2014) Comparative study of MPS method and level-set method for sloshing flows, *Journal of hydrodynamics* **26**(4), 577–585.

[24] Zhang, Y. L., Tang, Z. Y. and Wan, D. C. (2016) Numerical Investigations of Waves Interacting with Free Rolling Body by Modified MPS Method, *International Journal of Computational Methods* **13**(4), 1641013.

[25] Tang, Z. Y., Zhang, Y. L. and Wan, D. C. (2016) Multi-resolution MPS method for free surface flows, *International Journal of Computational Methods* **13** (4), 1641018.

[26] Zhang, Y. L. and Wan, D. C. (2017) Numerical study of interactions between waves and free rolling body by IMPS method, Computers and Fluids, https://doi.org/10.1016/j.compfluid.2017.03.019.

[27] Lee, B. H., Park, J. C., Kim, M. H., Jung, S. J., Ryu, M. C. and Kim, Y. S. (2010) Numerical simulation of impact loads using a particle method, *Ocean Engineering* **37**, 164–173.

[28] Newmark, N. M. (1959) A method of computation for structural dynamics, *Journal of the engineering mechanics division* **85**(3), 67–94.

[29] Hsiao, K. M., Lin, J. Y. and Lin, W. Y. (1999) A consistent co-rotational finite element formulation for geometrically nonlinear dynamic analysis of 3-D beams, *Comput. Methods Appl. Mech. Engrg* **169**, 1–18.